J. Phys.: Condens. Matter **20** (2008) 384203 (5pp) doi:10.1088/0953-8984/20/38/384203

THz operation of asymmetric-nanochannel devices

C Balocco[1], M Halsall[1], N Q Vinh[2] and A M Song[1]

[1] School of Electrical and Electronic Engineering, University of Manchester, Manchester M60 1QD, UK
[2] FELIX Free Electron Laser Facility, FOM Institute for Plasma Physics 'Rijnhuizen', PO Box 1207, NL-3430 BE Nieuwegein, The Netherlands

E-mail: A.Song@manchester.ac.uk

Received 14 March 2008
Published 21 August 2008
Online at stacks.iop.org/JPhysCM/20/384203

Abstract

The THz spectrum lies between microwaves and the mid-infrared, a region that remains largely unexplored mainly due to the bottleneck issue of lacking compact, solid state, emitters and detectors. Here, we report on a novel asymmetric-nanochannel device, known as the self-switching device, which can operate at frequencies up to 2.5 THz for temperature up to 150 K. This is, to our knowledge, not only the simplest diode but also the quickest acting electronic nanodevice reported to date. The radiation was generated by the free electron laser FELIX (Netherlands). The dependences of the device efficiency as a function of the electric bias, radiation intensity, radiation frequency and temperature are reported.

(Some figures in this article are in colour only in the electronic version)

1. Introduction

The terahertz region of the electromagnetic spectrum (1 THz = 1000 GHz = 10^{12} Hz) has been steeply gaining attention because of potential applications in both fundamental science and technology. The impact in threat-prevention systems has been impressive: concealed-weapons detection, explosive fingerprinting and remote trace detection of bio-particles are only a few of the applications in which academia and industry are deeply engaged [1–3]. THz radiation is also extensively studied in astrophysics, being one of the most interesting spectral features of the 2.7 K cosmic microwave background [4]. Furthermore, the development of compact ultra-scaled semiconductor devices operating at THz frequencies is paramount for matching the requirements of the next-generation information processing technology. Solid state detectors and emitters, which are compact and inexpensive, are believed to be the key to the future of THz technologies.

Nanostructures realized by patterning two-dimensional electron gases (2DEGs) in a compound semiconductor heterostructure seem to be promising candidates for high-speed applications. Song *et al* showed that ballistic rectifiers and nanostructured nonlinear materials, both having four terminals, could be used for microwave detection up to at least 50 GHz at room temperature [5–8]. Three-terminal ballistic junctions were also measured up to 1 GHz by Lewén *et al* [9] and up to 20 GHz by Worschech *et al* [10]. However, these multi-terminal nanodevices cannot be easily connected in parallel, to reduce the total impedance, unless an interconnection layer is used, which inevitably adds parasitic elements.

Recently, we demonstrated an ultra-fast novel electronic nanodevice, namely the self-switching device (SSD) [11, 12], which showed efficient detection of microwaves up to 110 GHz at room temperature [13]. The device, being both planar and requiring only a single lithographic step, is to our knowledge the simplest diode to date. Recently, Monte Carlo simulations predicted that the device could operate at frequencies up to a few THz (wavelength $\sim 100\ \mu$m) [14–16].

Here, we perform experiments on SSD arrays at THz frequencies using a free electron laser. At temperatures below 150 K, successful detection of free-space radiation has been achieved between 1.3 and 2.5 THz (wavelength 120–230 μm). This is, to the authors' knowledge, the quickest acting novel electronic nanodevice reported to date.

2. Self-switching device (SSD)

The SSD is realized by tailoring the boundary of a narrow semiconductor channel by means of two L-shaped trenches as

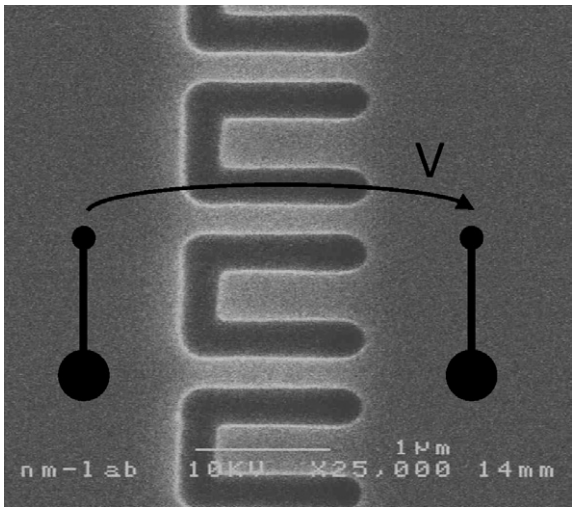

Figure 1. Scanning electron micrograph of an array of SSDs which are connected in parallel. The darker area is that of the trenches etched into the 2DEG.

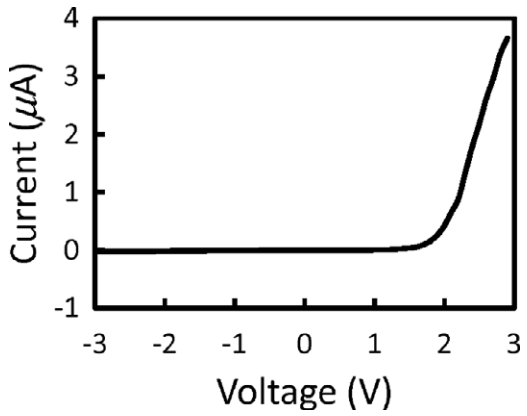

Figure 2. Current–voltage characteristic of an array of six SSDs connected in parallel and measured at room temperature.

shown in figure 1. A voltage applied over the channel V not only changes the potential profile along the channel direction, but also either widens or narrows the effective channel width, depending on its sign. With the device unbiased ($V = 0$), the effective channel width is almost pinched off by the surface states on the etched boundaries. A negative bias ($V < 0$) further depletes the channel, whereas a positive bias ($V > 0$) counteracts the lateral depletion, widening the effective width of the channel. This results in a strong nonlinear I–V characteristic, as shown in figure 2, resembling that of a conventional diode, but without using any doped junctions or any tunnelling barriers (details in [11]).

The threshold voltage is determined by the geometrical width of the SSD channel, rather than by the material. This adds flexibility, since devices with different turn-on voltages can be designed out of the same semiconductor substrate. The planar SSD layout permits the fabrication of simple circuits without using interconnection layers, minimizing the parasitic elements. For example, linear arrays of SSDs connected in parallel can be fabricated by simply placing SSDs next to each other. Moreover, by folding a linear array as many times as required, a large area, e.g., a whole wafer, can be turned into an active device.

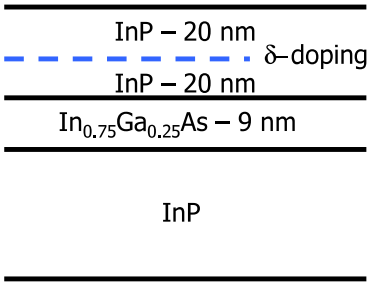

Figure 3. Structure of the wafer used to fabricate the SSD arrays. The 2DEG is confined in the 9 nm thick InGaAs quantum well located 40 nm below the surface.

The SSD can be modelled as a conventional field-effect transistor where its gate electrode has been short-circuited with its drain electrode. The simple treatment developed in [17] predicted for an SSD with a channel completely depleted by surface states a current proportional to the square of the applied voltage in forward bias over threshold, or zero otherwise, in very good agreement with the experiments. A more accurate description of the transport properties of SSDs, aided by Monte Carlo simulations, in both the AC and DC regimes, is in [14–16, 18].

3. Fabrication

The devices were fabricated out of an $In_{0.75}Ga_{0.25}As$/InP wafer, sketched in figure 3, in which free electrons were confined to a 2DEG in a 9 nm thick quantum well, located 40 nm below the surface. The carrier density and the electron mobility at $T = 4$ K were 4.5×10^{15} m^{-2} and 45 m^2 V^{-1} s^{-1}, respectively, as determined by Hall measurements. The active areas of the SSDs could be fabricated in just one high-resolution lithographic step, avoiding critical mask alignments and interconnection layers. All the devices were defined by EBL followed by an HBr-based wet etching. The ohmic contacts were formed by alloying Au/Ge/Au at 390 °C. Several arrays with a different numbers of elements and different layouts have been fabricated and tested. The SSD channels were 1.2 μm long, and 60–100 nm wide. The SSD arrays were etched in a 7 μm wide two-terminal mesa structure, which could accommodate up to six SSDs.

4. THz wave detection

Electronic devices with a nonlinear diode-like I–V characteristic, such as the SSD, can be used to rectify an AC input to a DC output. If the voltage across the diode is

$$V = V_0 + v_0 \cos \omega t, \tag{1}$$

where V_0 is the applied DC bias and v_0 is the amplitude of a small sinusoidal signal of frequency $f = \omega/2\pi$. The

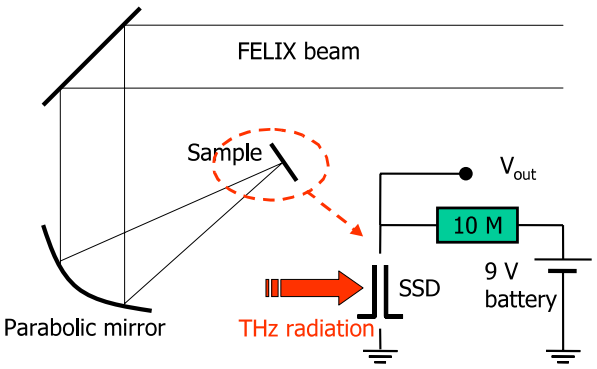

Figure 4. Set-up used to measure the response of SSDs illuminated by THz radiation. The FELIX beam is focused onto the SSDs by a parabolic mirror. The SSDs are biased through a resistor by a 9 V battery.

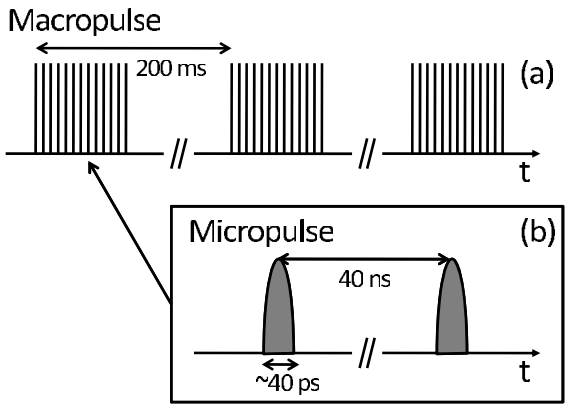

Figure 5. Structure of the macropulses (a), repeated every 200 ms (5 Hz rate), and micropulses (b), repeated every 40 ns (25 MHz rate), of the FELIX beam.

Taylor expansion leads to the small-signal approximation of the current [19]:

$$I = I_0 + v_0 G_d \cos\omega t + \frac{v_0^2}{2} G'_d \cos^2 \omega t + \cdots \tag{2}$$

$$= I_0 + \frac{v_0^2}{4} G'_d + v_0 G_d \cos\omega t + \frac{v_0^2}{4} G'_d \cos 2\omega t + \cdots, \tag{3}$$

where I_0 is the bias current, $G_d = \frac{\mathrm{d}I}{\mathrm{d}V}|_{V=V_0}$ the differential conductance, $G'_d = \frac{\mathrm{d}^2 I}{\mathrm{d}V^2}|_{V=V_0}$ the second derivative of $I(V)$ at $V = V_0$, also referred to as the bowing coefficient, and $\frac{v_0^2}{4} G'_d$ is the rectified DC current. In an open-circuit configuration the voltage across the device will be

$$\beta_v = \frac{v_0^2}{4} G'_d \frac{1}{G_d}. \tag{4}$$

Equation (4) shows how the detected open-circuit voltage is proportional to the power of the AC signal and the bowing coefficient, loaded on the device differential impedance.

Moreover, since all the SSDs were connected in parallel and worked simultaneously, the overall noise level was expected to be lower than in a single SSD, as can be determined with the following simple model. Let us assume that Δi is the rectified DC current flowing in a single SSD, and n_i the rms noise generated by a single SSD. The total current rectified by M SSDs, ΔI, is

$$\Delta I = M \times \Delta i, \tag{5}$$

and the total rms current noise N_i is

$$N_i = \sqrt{M \times n_i^2}. \tag{6}$$

The signal-to-noise ratio of the array $(\frac{S}{N})_{\mathrm{tot}}$ is

$$\left(\frac{S}{N}\right)_{\mathrm{tot}} = \frac{\Delta I}{N_i} = \frac{M \times \Delta i}{\sqrt{M \times n_i^2}} = \sqrt{M} \times \left(\frac{S}{N}\right)_{\mathrm{single}}, \tag{7}$$

where $(\frac{S}{N})_{\mathrm{single}}$ is the signal-to-noise ratio of a single SSD. The signal-to-noise ratio of the M-element array is hence $\sqrt{M}$ times higher than that of a single SSD.

We expect to improve significantly the microwave sensitivity and the frequency response flatness by optimizing our structures. Increasing the number of SSDs in the arrays will further reduce the impedance, helping reduce the time constants related to the parasitic capacitance, and improving the signal-to-noise ratio.

5. Measurement set-up

For our experiments we utilized the THz radiation generated in the European FEL facility FELIX (Free Electron Laser for Infrared eXperiments). During the measurement of the SSD response to the THz radiation, FELIX was operated in the spectral range 230 μm (~1.3 THz)–120 μm (2.5 THz), which was the wider continuously tunable range provided by FELIX FEL 1. The micropulse rate was kept constantly at 25 MHz. The average power of the macropulses was 1250 μW as measured by a pyrometer. The micropulse peak power was estimated to be approximately 50 kW. We note that the actual power that was effectively applied to the device was orders of magnitude lower because no device antenna was used. The SSD was cooled in a continuous-helium-flow cryostat with windows transparent at THz frequencies.

The set-up used to measure the SSD THz response is sketched in figure 4. FELIX's THz beam was focused onto the SSD array by a parabolic mirror. No antenna was used. The array was biased by a 9 V battery through a 10 MΩ resistor, which forced a current of 0.9 μA. Other bias currents were achieved by changing the resistor. The output voltage transient was recorded by a digital oscilloscope.

The time structure of the micropulses and macropulses of the FELIX beam is shown in figure 5. The width Δt of the micropulses was estimated from the linewidth of the laser at the wavelength λ with the approximate formula

$$\Delta t = \frac{\lambda^2}{\Delta\lambda(\%)} \times 0.147. \tag{8}$$

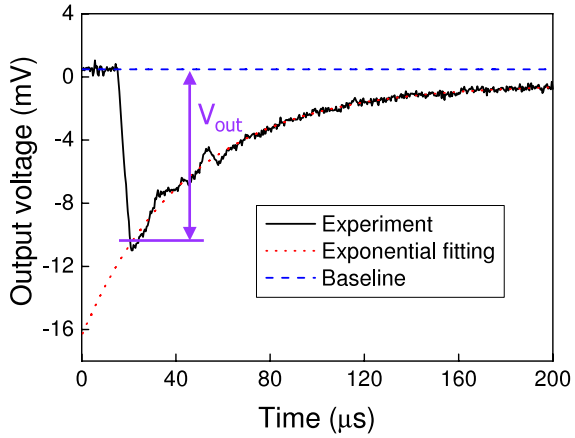

Figure 6. SSD output as detected by an oscilloscope (solid line). V_{out} is extracted by an exponential fitting of the transient (dotted line) and by a constant fitting of the baseline (dashed line).

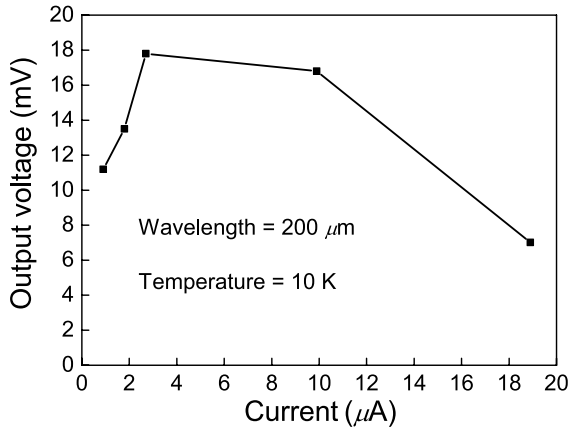

Figure 7. Detected voltage as a function of the current bias measured at 10 K. The radiation wavelength was 200 μm. The particular dependence reflects the nonlinearity of the device I–V characteristic.

6. Results and discussion

Figure 6 shows the electric signal detected by the SSD array. The first fast transient had a duration of about 10 μs, which is about the same as that of the macropulse. The second slow transient is believed to be determined by the parasitic RC time constant(s) of the electronic set-up. The detected voltage has been extracted by fitting the transient with an exponential function, in order to avoid artefacts due to the transient tail. The slow transient is well fitted by one exponential function, which suggests a single dominant RC time constant, probably due to the stray capacitance of the cryostat connections and the long cables from the cryostat to the oscilloscope.

The detected signal as a function of the current bias is shown in figure 7. Different DC currents were forced in the SSD array, which was cooled at 10 K, while the power of the THz beam was kept constant. The profile of the curve reflects the nonlinearity of the device I–V characteristic: the highest sensitivity was found when the array was fully turned on (approximately at 3 μA) as expected; as the current further increased, the I–V characteristic was linearized by the parasitic series resistance and the efficiency dropped.

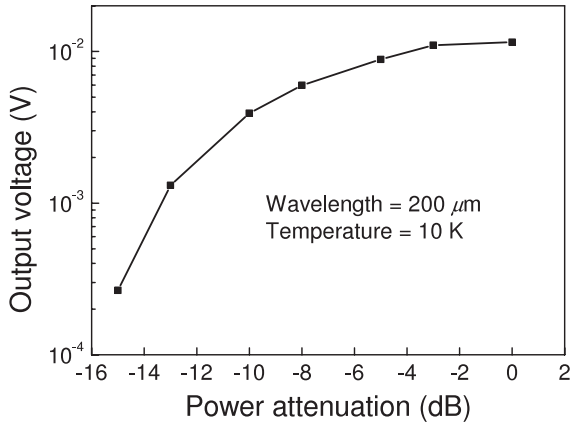

Figure 8. Detected voltage as a function of the beam attenuation measured at 10 K and at a wavelength of 200 μm. At 0 dB, the average macropulse power was 1250 μW. The actual power that was effectively applied to the device was much lower without using an antenna.

The detected signal as a function of the radiation power is shown in figure 8. The FELIX beam filters (3 dB, 5 dB, 10 dB), and their combinations, were used to attenuate the beam power. At 0 dB, the power was 1250 μW. Since such a low power was used, one would expect a linear relation between the detected DC voltage and the power (i.e., the device working in the square-law region). However, figure 8 shows a sub-linear dependence, which could be explained in the following way: when the high-power micropulse hits the sample a DC voltage across the device is induced, which drives the SSD array to a low-impedance region. After the micropulse is finished, the SSD array falls back in a relatively high-impedance region, and the stray capacitance holds the previously detected DC voltage; the decay is not observed because of the fast micropulse rate (40 ns or 25 MHz). The same process is repeated for the forthcoming micropulses. After the macropulse is finished, the held DC voltage has time to decay, as shown in figure 6. Following this model, we must now consider the peak power (approximately 50 kW), rather than the average power. It is worth pointing out that only a small fraction of the THz power was actually effectively applied to the SSD array since no antenna was used. Nevertheless the power could not be regarded as 'low', and it seems to be reasonable that the SSD array was driven away from the square-law region.

Figure 9 shows the detected voltage as a function of the radiation wavelength, ranging from 120 μm (2.5 THz) to 230 μm ($\sim$1.3 THz) with the sample cooled at 10 K. The dotted trace is the beam power measured by a pyrometer, whereas the solid trace is that detected by the SSD array. Since the relation between detected voltage and power is not linear, it is not possible to normalize the detected signal. However, the signal from the SSD array followed very well the features of the beam power, with a slight efficiency drop, as expected, at the lower wavelengths.

Finally, the detected signal as a function of the temperature was measured, and the results are reported in figure 10. Radiation at 200 μm was detected up to 150 K. The reduction of the detected voltage at temperatures above 60 K can be caused by the reduction of the mobility of the 2DEG confined in the $In_xGa_{1-x}As$ quantum well [20].

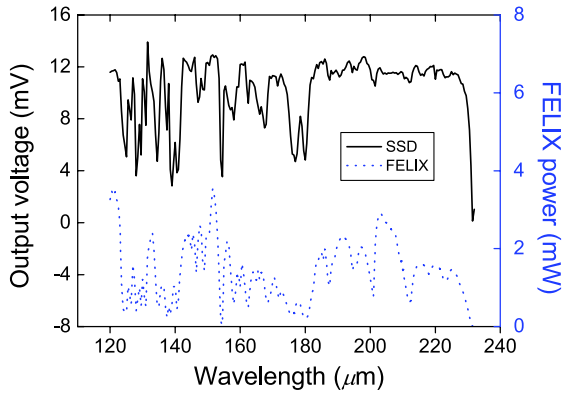

Figure 9. Detected voltage as a function of the wavelength at 10 K (solid line). The power of FELIX beam as measured by a pyrometer (dotted line).

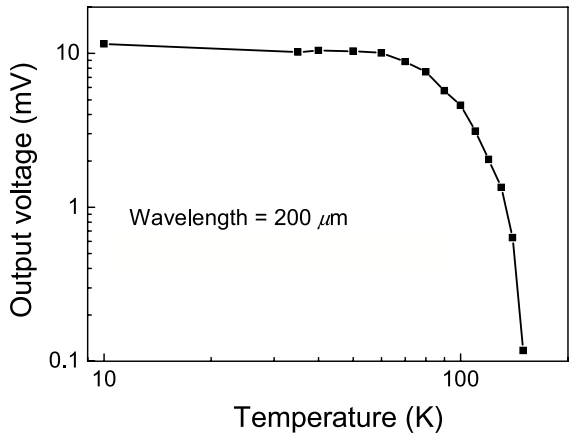

Figure 10. Dependence of the detected voltage as a function of the temperature.

7. Conclusions

Frequencies up to at least 2.5 THz have been detected at temperatures below 150 K. However, operation at higher temperatures, as envisaged by simulations [14, 15], has not been excluded, since the signal-to-noise ratio of the measurement set-up can be greatly enhanced. In particular, the use of a lock-in amplifier, rather than digital sampling through an oscilloscope, would dramatically improve the ultimate signal-to-noise ratio. Fabrication of larger SSD arrays will lead to a lower impedance and a higher signal-to-noise ratio, and we have already demonstrated the feasibility of arrays with up to 100 SSDs.

Acknowledgments

This work was supported by the Engineering and Physical Science Research Council (EPSRC), the Royal Society, and the European Community—Research Infrastructure Action under the FP6 'Structuring the European Research Area' Programme through the Integrated Infrastructure Initiative 'Integrating Activity on Synchrotron and Free Electron Laser Science'. We gratefully acknowledge the support by the Stichting voor Fundamenteel Onderzoek der Materie (FOM) in providing the required beam time on FELIX and the skilful assistance by the FELIX staff.

References

[1] Hu B B and Nuss M C 1995 *Opt. Lett.* **20** 1716
[2] Sherwin M 2002 *Nature* **420** 131
[3] Chen Q and Zhang X C 2001 *Ultrafast Lasers: Technology and Applications* ed M E Fermann, A Galvanauskas and G Sucha (New York: Dekker)
[4] de Bernardis P *et al* 2000 *Nature* **404** 955
[5] Song A M, Lorke A, Kriele A, Otthaus J P, Wegscheider W and Bichler M 1998 *Phys. Rev. Lett.* **0** 3831
[6] Song A M 1999 *Phys. Rev.* B **59** 9806
[7] Song A M, Omling P, Samuelson L, Seifert W, Shorubalko I and Zirath H 2001 *Japan. J. Appl. Phys.* **40** L909
[8] Song A M, Omling P, Samuelson L, Seifert W, Shorubalko I and Zirath H 2001 *Appl. Phys. Lett.* **79** 1357
[9] Lewén R, Maximov I, Shorubalko I, Samuelson L and Thylén L 2001 *J. Appl. Phys.* **91** 2398
[10] Worschech L, Fischer F, Forchel A, Kamp M and Schweizer H 2001 *Japan. J. Appl. Phys.* **40** L867
[11] Song A M, Missous M, Omling P, Peaker A R, Samuelson L and Seifert W 2003 *Appl. Phys. Lett.* **83** 1881
[12] Song A M, Missous M, Omling P, Peaker A R, Samuelson L and Seifert W 2005 *Appl. Phys. Lett.* **86** 042106
[13] Balocco C *et al* 2005 *Nano Lett.* **5** 1423
[14] Mateos J, Song A M, Vasallo B G, Pardo D and González T 2005 *Proc. SPIE* **5838** 145
[15] Mateos J, Vasallo B G, Pardo D and González T 2005 *Appl. Phys. Lett.* **86** 212103
[16] Xu K Y, Lu X F, Song A M and Wang G 2008 *J. Appl. Phys.* **103** 113708
[17] Åberg M, Saijets J, Song A M and Prunnila M 2004 *Phys. Scr.* T **114** 123
[18] Xu K Y, Lu X F, Wang G and Song A M 2008 *IEEE Trans. Nanotechnol.* at press
[19] Pozar D M 1998 *Microwave Engineering* 2nd edn (New York: Wiley)
[20] Ng G I *et al* 1988 *Appl. Phys. Lett.* **52** 728